JOURNAL OF GEOPHYSICAL RESEARCH, VOL. 115, A07216, doi:10.1029/2009JA014971, 2010

Click Here for Full Article

# Asymmetries in Saturn's radiation belts

C. Paranicas,[1] D. G. Mitchell,[1] S. M. Krimigis,[1] J. F. Carbary,[1] P. C. Brandt,[1] F. S. Turner,[1] E. Roussos,[2] N. Krupp,[2] M. G. Kivelson,[3] K. K. Khurana,[3] J. F. Cooper,[4] T. P. Armstrong,[5] and M. Burton[6]

Received 7 October 2009; revised 6 January 2010; accepted 24 February 2010; published 17 July 2010.

[1] We present both energetic proton and electron data from the main radiation belts of Saturn. When organized by L shell and equatorial pitch angle, data from Cassini's Magnetospheric Imaging Instrument reveal proton radiation belts that are highly symmetric in local time. The energetic electron radiation belts are asymmetric in two principal ways. Using data from two close passes of the planet, we find for energies near a few MeV, electron intensity levels are different between noon and midnight. Furthermore, when Cassini was inbound to Saturn, electron fluxes dropped precipitously before the spacecraft reached the main rings. Outbound, electron fluxes returned to high levels when the spacecraft moved outward of the main rings. In this paper, we suggest that electron flux level asymmetries are due in part to the presence of local time stationary particles in Saturn's inner magnetosphere. We also consider possible mechanisms to account the drop off of electrons near the ring edge on the dayside.

**Citation:** Paranicas, C., et al. (2010), Asymmetries in Saturn's radiation belts, *J. Geophys. Res.*, *115*, A07216, doi:10.1029/2009JA014971.

## 1. Introduction

[2] Each of the magnetospheres of the outer planets contains intense regions of stably trapped energetic charged particles. At Saturn, these radiation belts are most intense between the outer edge of the main rings ($R \sim 2.27\ R_S$; $1\ R_S = 60{,}268$ km) and Enceladus's orbit ($R \sim 3.95\ R_S$). Modeling of these belts has reproduced many of their salient features [e.g., *Santos-Costa et al.*, 2003]. Prior to Cassini, in situ measurements of Saturn's radiation belts were made during the flybys of three spacecraft with closest approach distances of 1.35 $R_S$ (Pioneer 11), 3.07 $R_S$ (Voyager 1) and 2.67 $R_S$ (Voyager 2). Cassini had a closest approach distance of 1.33 $R_S$ during Saturn Orbit Insertion (SOI) on July 1, 2004. Cassini crossed over the main rings at about noon local time (LT) and exited the rings just before midnight (LT). Several subsequent Cassini periapses were within the radiation belts [*Burton et al.*, 2009] but to date have not revisited the region immediately adjacent to the main rings. While the radiation belts are thought of as fairly stable in time, Cassini data have revealed transient components. *Roussos et al.* [2008] discovered a radiation belt in early 2005 that extended approximately from the orbit of Tethys ($R \sim 4.89\ R_S$) to 8 $R_S$. This transient radiation belt was observed to decay in intensity on later orbits. In this paper, we will report on the innermost portions of the electron and proton radiation belts and their observed structure in local time.

[3] During SOI, the proton radiation belts of Saturn were observed to be symmetric in the noon-midnight meridian [*Paranicas et al.*, 2008], using data from the Magnetospheric Imaging Instrument (MIMI). We found the energetic proton fluxes dropped to background levels close to the planet (inward of about 2.37 $R_S$). Later Cassini orbits also showed highly organized MeV proton belts [*Krupp et al.*, 2009]. But, as we will illustrate in this paper, the electron belts are observed to be asymmetric in a number of ways. The electron belts (both in the MeV and down to the hundreds of keV energy range) do not extend to the edge of the main rings on the inbound leg of the Cassini pass on SOI, but do on the outbound leg. Furthermore, even when the data are organized by L shell and equatorial pitch angle, the inbound/outbound intensities are very different. A similar flux asymmetry in the few MeV electrons was also observed during the Pioneer 11 flyby [e.g., *Simpson et al.*, 1980]. The Pioneer 11 trajectory came close to the outer edge of the main rings between noon and dusk inbound to the planet and between midnight and dawn outbound.

[4] In this paper, we will present Cassini data from the inner radiation belts. We will also look at the motion of trapped particles in that region. We will focus specifically on two issues. The first is the level of inbound/outbound flux level symmetry in different energy bands. The second is the reason

[1]Johns Hopkins University Applied Physics Laboratory, Laurel, Maryland, USA.
[2]Max-Planck-Institut für Sonnensystemforschung, Katlenburg-Lindau, Germany.
[3]IGPP, UCLA, Los Angeles, California, USA.
[4]NASA GSFC, Greenbelt, Maryland, USA.
[5]Fundamental Technologies, LLC, Lawrence, Kansas, USA.
[6]JPL, California Institute of Technology, Pasadena, California, USA.

Copyright 2010 by the American Geophysical Union.
0148-0227/10/2009JA014971

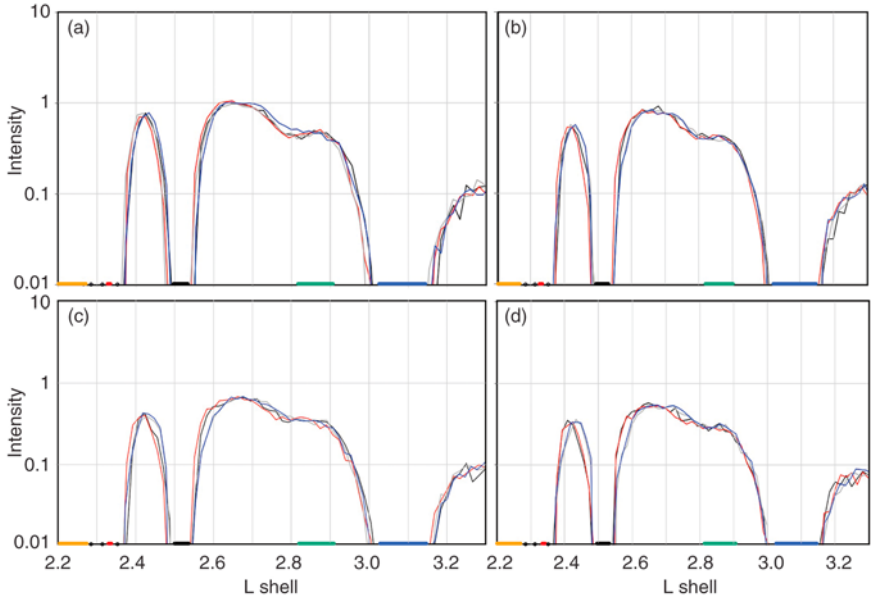


**Figure 1.** Intensities (counts per cm$^2$-s-sr-keV) of 2.28 – 4.49 MeV protons as a function of dipole L shell during SOI. Data obtained when the spacecraft was inbound to Saturn are displayed as red and black curves and outbound data are represented by gray and blue curves. Different pitch angle bins are plotted separately: (a) 11.25° and 168.75°, (b) 33.75° and 146.25°, (c) 56.25° and 123.75°, and (d) 78.75° and 101.25°. From the left edge of the horizontal axis at L = 2.2 the following markers are shown: the A ring (orange), some small satellites, the F ring (red), the sweeping corridor of Janus in black near L = 2.5, the G ring (green) and the sweeping corridor of Mimas in blue near L = 3.1.

for the absence of electrons on the dayside in the region of space just beyond the outer edge of the main rings.

## 2. Data

[5] In Figure 1, we show the intensities (counts per cm$^2$-s-sr-keV) of 2.28–4.49 MeV protons from MIMI's low energy magnetospheric measurements system (LEMMS) sensor [*Krimigis et al.*, 2004]. These data were obtained during SOI on days 2004–182 and 2004–183. We have used a dipole model of the magnetic field with a northward offset of 2,230 km along the spin axis of the planet [*Dougherty et al.*, 2005] to compute the L shell and equatorial pitch angle at each point. For Figure 1, data were binned by their equatorial pitch angle, $\alpha_{eq}$. Figure 1a shows the most field-aligned particles with Figures 1b–1d showing more equatorial particles. Line colors are as follows: black (spacecraft inbound to Saturn, particle $\alpha_{eq} < 90°$), red (inbound, $\alpha_{eq} > 90°$), gray (outbound, $\alpha_{eq} < 90°$), and blue (outbound, $\alpha_{eq} > 90°$). The range of L shells encountered by the moons Janus and Mimas are indicated on the plot. The satellite positions were determined using the information in SPICE (see http://naif.jpl.nasa.gov/naif/) for the period around SOI and then these positions were used to approximate each satellite's full excursion in L shell (for more details, see *Paranicas et al.* [2008]). Moons of all sizes can efficiently remove trapped energetic protons from the inner magnetosphere of Saturn. Therefore, we do not focus on the causes of the structure of the proton belts in this paper.

[6] It is clear from Figure 1 that the points obtained on the inbound/outbound legs of the trajectory are highly symmetric when organized by L shell and equatorial pitch angle. It is noteworthy that proton intensities peak in the most field-aligned direction. For instance, the peak intensities in Figures 1a–1d, from the most field-aligned to least field-aligned fluxes, are about 1.0, 0.8, 0.7, and 0.5 counts per cm$^2$-s-sr-keV. *Armstrong et al.* [2009] have analyzed and interpreted various types of energetic ion pitch angle distributions observed in Saturn's inner magnetosphere. We therefore do not focus on the details of the pitch angle distributions in this work.

[7] For protons with $\alpha_{eq} = 75°$ near the A ring edge, the time to complete a rotation of Saturn in inertial space is 5.2 h (2 MeV) and 3.4 h (4 MeV), where we assume rigid corotation and gradient-curvature drift in the dipole field. We note further that the strong variation in the drift rate with energy occurs for all particle pitch angles. Therefore, however these particles are transported/energized, they would be expected to rapidly disperse in longitude.

[8] In Figure 2, we present 1.6 – 21.0 MeV electron data taken by LEMMS during SOI. The raw data are processed in the same manner as was used for the proton data. As in Figure 1, each plot in Figure 2 represents a separate equatorial pitch angle bin with the most field-aligned particles displayed in Figure 2a. Figures 2b–2d show particles with larger equatorial pitch angles. Here are some points of note in Figure 2. The moon absorptions are not as pronounced in electron fluxes as they are in the energetic protons (see discussions by, e.g., *McDonald et al.* [1980] and *Roussos et al.* [2007]). Particles traveling parallel and anti-parallel to the magnetic field line have comparable fluxes (e.g., the red and black lines in Figure 2a). The flux levels are usually highest

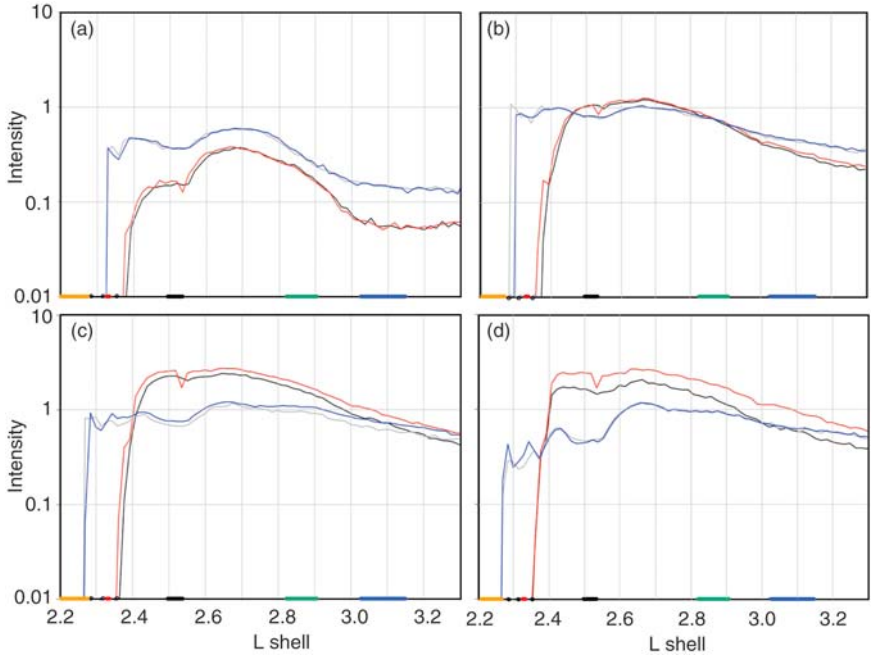


**Figure 2.** Intensities (counts per cm$^2$-s-sr-keV) of 1.6 – 21 MeV electrons as a function of L shell during SOI. The four plots represent averages in different equatorial pitch angle bins and the color scheme, etc., is exactly as it is in Figure 1.

for equatorially mirroring particles. The overall flux levels of the particles with the same pitch angles measured on the inbound and outbound legs of the trajectory are not the same (e.g., the red versus blue curve in Figure 2a).

[9] Regarding differences among pitch angles, the inbound data begin to drop off at about L = 2.38 in all the pitch angle bins. On the outbound leg, the flux levels return to high values at different radial distances from the planet. The particles mirroring closest to the magnetic equator return to high flux first at L ~ 2.27. The most field-aligned particles return to high levels at L ~ 2.33. We have not identified ways in which the Saturn kilometric radiation (SKR) phase would be likely to affect these fluxes, but it might prove useful to note that the SKR longitudes differed on the inbound and outbound passes, with the inbound trajectory crossing the main ring edge near 310°W and the outbound crossing near 250°W [*Kurth et al.*, 2007].

[10] Several other LEMMS electron channels spanning energies from about 110 keV to more than 7 MeV closely follow the behavior of the channel displayed in Figure 2 near the rings. Also, the inbound drop off of flux occurred close to a spacecraft maneuver that oriented the high gain antenna into the plasma ram direction. To confirm that this did not affect our measurements, we analyzed the background counts in the MIMI charge-energy-mass spectrometer (CHEMS). This sensor's singles rates (bare detector rates ignoring coincidence) are a proxy for energetic electron penetrators at these distances. We found that the LEMMS foreground signal was well correlated with the CHEMS singles rates, suggesting to us that the electrons were indeed absent inbound.

[11] In Figure 3, we show another Cassini pass (April 14–15, 2005) through the radiation belts. Here we plot both proton and electron channels on the same graph as a function of L shell. Plotted are 0.79–4.75 MeV electrons (black), 1.6–21.0 MeV electrons (red), and 2.28–4.49 MeV protons (blue). The lines corresponding to lower fluxes were taken during the inbound portion of the trajectory. At this point in the mission, LEMMS was no longer reporting full pitch angle distributions, so these intensities correspond at each point to a fixed pitch angle determined by the relative angle between LEMMS and the magnetic field at that time. In the radiation belts, these electron intensities are a stronger function of pitch angle than the proton intensities and therefore show a more pronounced change during spacecraft maneuvers, when the sensor is sampling different pitch angles as it moves. *Roussos et al.* [2007] have also provided some analysis of this time period focusing on the region around Mimas's orbit. This Cassini orbit occurred close to the planetary equatorial plane, the inbound/outbound latitudes have approximately the same absolute values, and the inbound/outbound pitch angle sampling was very similar. The inbound and outbound electron fluxes shown in Figure 3 are very similar around periapsis, R ~ 2.6 $R_S$. Here the spacecraft covered a local time range between about 16:15 and 22:00 inside of L = 3.

[12] The pattern of asymmetry shown here has some features in common with that found in the flux of Pioneer 11 electrons of roughly the same energies. *Van Allen and Grosskreutz* [1989] found that the fluxes of electrons detected when the spacecraft was inbound to Saturn were more intense than the outbound ones and these fluxes detected inbound fell off very quickly through the F ring region (R ~ 2.33 $R_S$). The qualitative shape of the fit they created to the inbound Pioneer 11 data agrees fairly well with the Cassini data taken on the inbound at similar energies.

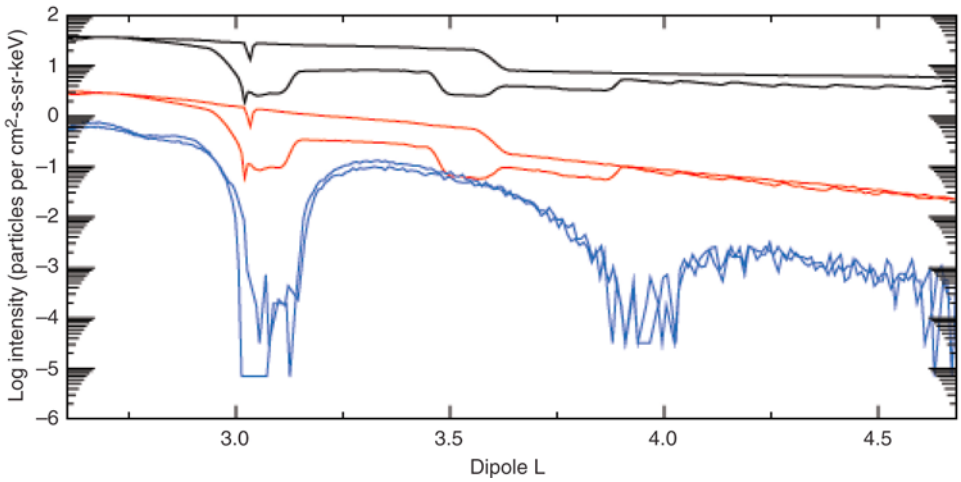


**Figure 3.** Proton (blue line) and electron (red and black lines) data obtained between 2005 and 104 18:30 UTC and 2005–105 04:00 UTC. These data are not all at the same equatorial pitch angle so some variations are due to the pitch angle distribution of the particle type. Inward of about L = 3, the local time range is 16:15 to 22:00.

Their interpretation was that this fall-off was the more typical situation in the inner magnetosphere and that the lower Pioneer 11 outbound intensities were due to temporal effects. An important difference between the two data sets is that the outbound Pioneer 11 flux increased gradually from the main ring edge. On Cassini, some fluxes return immediately to a high level beyond the ring edge and then remain fairly constant. Neither of the Voyager spacecraft crossed the ring plane close enough to the planet to measure the electrons just off the A ring.

## 3. Flux Asymmetries

[13] The differences in inbound/outbound intensities may have many sources and in this section we consider this issue. At Saturn, electrons gradient-curvature drift in a direction that is opposite to the plasma flow direction. At low energies, electrons have net motion in the same direction as that of the plasma flow and of all of the ions. However, at high enough energies, electron guiding-centers have net motion that is in the opposite direction to the plasma flow [e.g., *Thomsen and Van Allen*, 1980]. Here, we will call the energy at which electrons begin to have net longitudinal motion in the direction opposite to the corotational plasma flow the "transitional energy." *Roussos et al.* [2007] provide a plot of this energy with some pitch angle dependence, assuming rigid corotation. These transitional energies are about 1 MeV at Dione's orbit ($R \sim 6.26\ R_S$) and increase inward to approximately 3 MeV at the edge of the main rings. *Cooper et al.* [1998] have previously analyzed local-time stationary electrons in the ring current region of Saturn. They computed closed, banana-shaped orbits that were not circumplanetary, at Saturn distances between 8 and 16 $R_S$. It follows from that analysis that at each radial distance from Saturn, there will be a population of electrons whose guiding centers will not sample all local times. If electrons are not energized in exactly equal numbers around the whole drift shell, asymmetries will be present. Therefore spacecraft detectors with wide energy passbands (e.g., that bracket some of the transitional energies or are affected by background electrons at these energies) should measure different intensities at different local times. In other words, if the source of these particles confines them in longitude, for instance, as injections or other processes [*Randall*, 1994] could, electrons near the transitional energy range could maintain such asymmetric distributions for long periods of time.

[14] To provide further evidence that the fluxes of particles with energies near the transition are the most asymmetric, we present another energy range for comparison. In Figure 4, we present 220 to 485 keV electrons from SOI. These are binned in exactly the same manner as in Figures 1 and 2. Electrons near L = 3 at energies of 220 keV and 485 keV with $\alpha_{eq} = 60°$, take 12.4 h and 14.4 h to complete an orbit of Saturn. Therefore, even if the source mechanism that accelerates electrons to these energies initially leads to fluxes that are asymmetric in local time, these asymmetries cannot be sustained. Such a picture is consistent with the data shown in Figure 4. That is, except in the region near the main rings, the data reveal that these lower energy electrons do have more symmetric fluxes in local time. By comparison, the electron fluxes depicted in Figure 2 are dominated by 1.6–4 MeV electrons. Electrons with energies of a few MeV are near the transitional range and do not disperse quickly on the drift shell. Therefore if the source of these few MeV electrons does not produce symmetric populations in local time, it will take longer for symmetric populations to develop by dispersion.

[15] Next we turn our attention to the process of energization. It is the conventional view of radiation belts that they form gradually over time and their structure evolves slowly. A great deal of acceleration to radiation belt energies can occur during inward radial transport. Other processes have been suggested that produce particles at radiation belt energies [e.g., *Randall*, 1994], but here we will examine the consequences of inward transport. Close to the planet, the inward radial transport is probably dominated by diffusion.

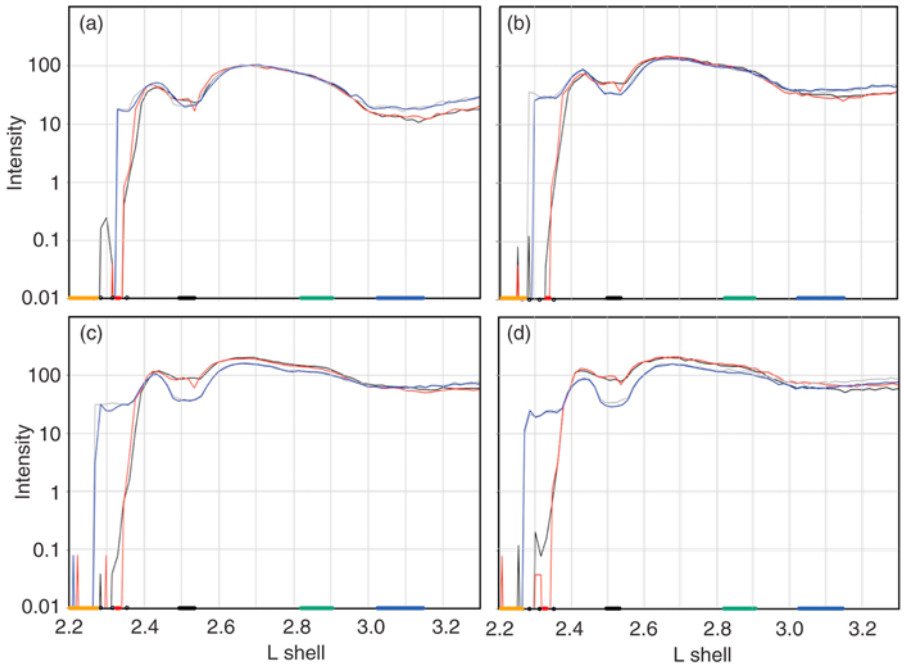


**Figure 4.** Intensities (counts per cm$^2$-s-sr-keV) of 220–485 keV electrons obtained by MIMI during SOI. Data are binned in the exact same manner as Figures 1 and 2, with the most field-aligned particles in the top left and the most equatorial particles in the bottom right.

To examine how this will influence local-time stationary structures, we consider transport where the first two adiabatic invariants of motion are conserved. *Kaufmann* [1965] has provided a relativistic formulation of the adiabatic invariants appropriate to MeV electrons. In both Figures 5 (top) and 5 (bottom), we show the change in energy for electrons that conserve $\mu$ and J in a dipole field at Saturn. To create these curves, we have used the following conditions. At L = 2.3, we assume a final energy of 3.15 MeV and final equatorial pitch angle of 60° (Figure 5, top) and 90° (Figure 5, bottom). These values were chosen to correspond to the local time stationary electrons at the main ring edge. At any other L in Figure 5, we compute the energy and pitch angle the particle would have to reach the ring edge with the above energy and pitch angle, assuming it conserves $\mu$ and J in a dipole field. The solution energy is the lowest curve in Figures 5 (top) and 5 (bottom) (triangles joined by a solid line). For J > 0 particles, we also plot the equatorial pitch angle at each L (circles joined by a line) that corresponds to the ones at the ring edge, assuming conservation of invariants. For the J ≈ 0 case in Figure 5 (bottom), the equatorial pitch angle does not vary appreciably with L. In Figures 5 (top) and 5 (bottom), for comparison, we also show the energy for electrons with the estimated pitch angle at each L to be stationary in local time (solid line). Electrons with energies close to the transitional energy drift slowly in longitude. This implies that a localized increase in flux would disperse slowly over the drift shell. As electrons are energized by inward transport processes, the nearly resonant electrons do not diverge from the resonance curve but instead track it. This means that the source population of resonant electrons is nowhere very far from the local time stationary curve. That is, as electrons are being energized to radiation belt energies, there is no place in the inner magnetosphere where these electrons are dispersing rapidly on the drift shell.

## 4. Trapped Electrons Near the Edge of the Main Rings

[16] The main rings of Saturn are nearly perfect absorbers of energetic charged particles. It is therefore worth considering whether the steep drop in electron fluxes during Cassini's inbound pass (Figures 2 and 4) prior to its reaching the ring edge can be due to the electron drift paths intersecting the rings at a local time remote from that of the spacecraft. In a dipole field, the guiding center drift paths in the equatorial plane are circles centered on the dipole. In the case of no electric fields, the conservation of the first adiabatic invariant means that particles mirroring near the equator will follow contours of constant B. If the dayside magnetosphere is compressed by the solar wind, these contours are closest to the planet near local midnight and farthest from the planet near local noon [e.g., *Walt*, 1994]. In such a picture, an equatorial drift trajectory could intersect the main rings in the midnight sector and be radially outward from the rings near noon.

[17] For very energetic electrons at Saturn (e.g., whose net motion is strongly retrograde), the net motion is guided by the magnetic field and it is a good approximation to assume the electric field is negligible. *Schulz and Lanzerotti* [1974] provide a more detailed discussion of this point for Earth's radiation belts in their introductory chapter. Then if B = constant contours intersect the ring near midnight but not noon, such a picture of the drift paths would provide a plausible explanation for the flux decreases in the very energetic electron data.

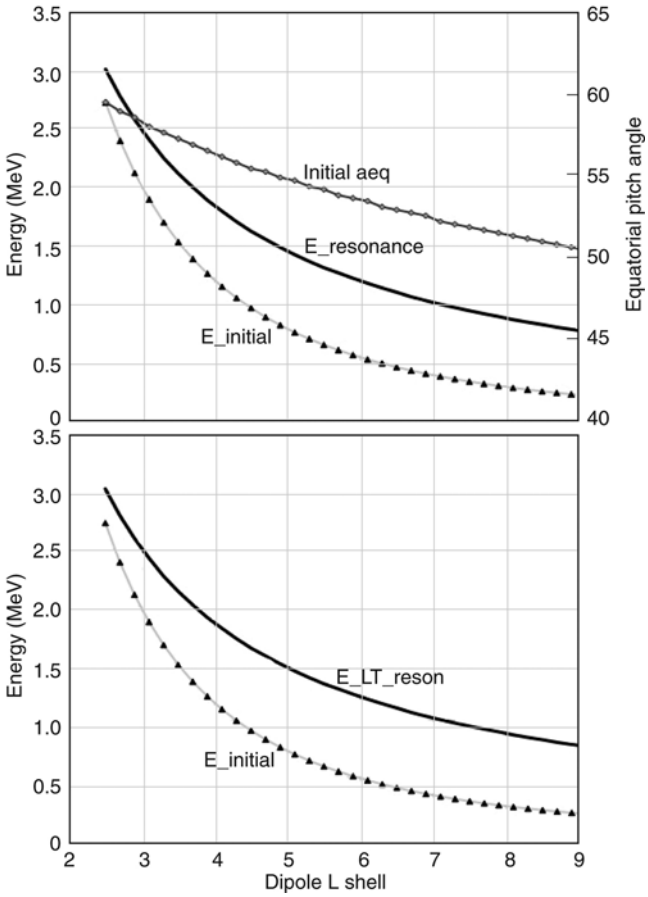


**Figure 5.** Mu-J energization curves for relativistic electrons. The lowest curves plot energy versus L shell if $\mu$ and J are conserved in a dipole field. (top) Electrons that mirror high above the magnetic equator. Its right-hand axis shows the equatorial pitch angle at each L shell corresponding to a fixed value of $\mu$ and J. (bottom) J ~ 0 particles. Each solid line with no tick marks indicates the L versus energy curve of electrons that are stationary in local time.

[18] For lower energy electrons detected by MIMI, the electric fields start becoming more important. Below about 2–3 MeV, the net guiding center motion is in the same direction as the cold plasma. The drift paths of the lower energy electrons would have common features with the protons (which are completely symmetric). So qualitatively we would expect equatorial electron drift paths to follow B = constant contours at the highest energies and progressively shift toward the cold plasma contours as energy decreases. However, Figures 2 and 4 show the drop-off near noon to be at exactly the same radial distance for both ranges of electron energies. This indicates to us that distortion of B = constant contours due to solar wind compression of the dayside could explain the data shown in Figure 2. But for this picture to explain the data shown in Figure 4, the electron intensities measured near the main rings would have to be dominated by higher energy electrons (i.e., electrons not in the nominal energy passband of the channel presented in Figure 4).

[19] Since most of MIMI's electron data are near or below the transitional energy near the main rings, it is also worth considering more quantitatively the effects of a global electric field, as previously suggested for Saturn by *Cooper et al.* [1998]. To model the electron drift paths near the main rings, we follow *Chen* [1970], who performed a similar calculation for Earth. *Chen* [1970] looked at particle drifts paths resulting from drifts, $v = E \times B/B^2$, where E is an effective electric field that can be written as the gradient of a generalized potential, $E = -\nabla\Phi$. Adapted for relativistic electrons in Saturn's inner magnetosphere, a similar potential can be written as,

$$\Phi = \frac{\Omega B_o R_S^2}{L} + \frac{mc^2}{q}\left[\left(\frac{2\mu B}{mc^2}+1\right)^{1/2} - 1\right] + E_o L R_S \sin\vartheta$$

Here $\Omega = 1.62 \times 10^{-4}$ rad/s, $B_o = 2.1 \times 10^{-5}$ T is chosen to correspond to the planetary dipole, and $E_o = 2 \times 10^{-5}$ V/m points from dusk to dawn, taken from the estimate by *Cooper et al.* [1998]. Such an electric field in Saturn's tail would lead to sunward convection of the plasma. Cylindrical coordinates are used as by *Chen* [1970] and the z axis is oriented along the spin axis of the planet. The potential above is valid in the z = 0 plane only for 90° pitch angle particles and $\theta$ is the angle from the sun direction increasing toward dusk. The first term corresponds to corotation, the second to the gradient drift and the third term to the convective electric field. By solving the equation, $\Phi = \Phi_o$, where $\Phi_o$ is an adjusted constant, a guiding center drift path in the z = 0 plane can be found as a function of $\theta$ and L.

[20] For the convective electric field above, we find that most particle orbits are circles whose centers are offset from Saturn's center toward dusk. The sense of the offset of the drift paths is consistent with the work of *Barbosa and Kivelson* [1983] on Jupiter. For lower energy particles, the centers of the equatorial drift paths shift duskward. For electrons near the energy transition (where the gradient drift begins to dominate over the corotation drift), the circles are offset by a larger amount and then at higher energies undergo a transition so that they are shifted toward dawn. To reproduce our data, we require the drift paths to be shifted toward noon (not dawn or dusk). Furthermore, a shift of 0.09 $R_S$ in our calculation corresponds to an electric field of at least $5 \times 10^{-4}$ V/m pointing from noon to midnight. The radial shift is estimated as follows. The inbound distance of the drop-off of electrons is L ~ 2.38, whereas the return to high flux is from L ~ 2.27 to 2.33, depending on pitch angle. Previously, *Roussos et al.* [2007] predicted an electric field of approximately this same noon-midnight orientation with a magnitude of at least $1 \times 10^{-4}$ V/m to explain displacements of microsignatures of Tethys and Dione. *Hedman et al.* [2007] also found a displacement of an absorption in radial distance from Saturn in the region of the G Ring.

[21] To reproduce the data with a steady state convective electric field, a higher field magnitude than that estimated by *Cooper et al.* [1998] is needed. Furthermore, partially rotating the electric field away from the noon-midnight direction toward the more likely dawn-dusk direction requires even higher field strengths to reproduce the asymmetry. Finally, the >7 MeV electron channel (not shown), whose behavior

just off the main rings is very similar to the electron channels presented above, is less sensitive to electric fields.

## 5. Conclusions

[22] Data from the main radiation belts of Saturn have been presented, focusing on the differences between the electron and proton belts. The intensities of protons and lower energy electrons do not appear to be strongly dependent on local time. We believe the rapid corotation of the low energy electrons and all the protons disperses them quickly on drift shells and local time asymmetries are therefore hard to sustain. This is not true of the few MeV electrons that can remain nearly stationary in local time and populate their drift shells in a non-uniform manner. The other aspect of the electron radiation belts that we considered here is the absence of energetic electrons just outward of the edge of the main rings in the dayside magnetosphere. By considering a dusk-to-dawn electric field, we could not reproduce this feature in the data. Very energetic electrons could populate the region just outward of the main rings on the nightside but not the dayside if their equatorial drift paths (contours of constant B) are not concentric with the main rings but shifted slightly toward the sun. For this effect to explain all the MIMI electron data, the lower energy electron channel presented above would have to be dominated by electrons above its nominal energy passband. We plan to pursue this issue in future work.

[23] **Acknowledgments.** We acknowledge useful conversations with F. Crary.

[24] Masaki Fujimoto thanks the reviewers for their assistance in evaluating this paper.

## References

Armstrong, T. P., et al. (2009), Energetic ions trapped in Saturn's inner magnetosphere, *Planet. Space Sci.*, *57*, 1723–1731, doi:10.1016/j.pss.2009.03.008.

Barbosa, D. D., and M. G. Kivelson (1983), Dawn-dusk electric field asymmetry of the Io plasma torus, *Geophys. Res. Lett.*, *10*, 210–213, doi:10.1029/GL010i003p00210.

Burton, M. E., M. K. Dougherty, and C. T. Russell (2009), Model of Saturn's internal planetary magnetic field based on Cassini observations, *Planet. Space Sci.*, *57*, 1706–1713, doi:10.1016/j.pss.2009.04.008.

Chen, A. J. (1970), Penetration of low-energy protons deep into the magnetosphere, *J. Geophys. Res.*, *75*, 2458–2467, doi:10.1029/JA075i013p02458.

Cooper, J. F., E. C. Sittler Jr., S. Maurice, B. H. Mauk, and R. S. Selesnick (1998), Local time asymmetry of drift shells for energetic electrons in the middle magnetosphere of Saturn, *Adv. Space Res.*, *21*, 1479–1482, doi:10.1016/S0273-1177(98)00022-2.

Dougherty, M. K., et al. (2005), Cassini magnetometer observations during Saturn orbit insertion, *Science*, *307*, 1266–1270, doi:10.1126/science.1106098.

Hedman, M. M., et al. (2007), The source for Saturn's G ring, *Science*, *317*, 653–656, doi:10.1126/science.1143964.

Kaufmann, R. L. (1965), Conservation of the first and second adibatic invariants, *J. Geophys. Res.*, *70*, 2181–2186, doi:10.1029/JZ070i009p02181.

Krimigis, S. M., et al. (2004), Magnetosphere imaging instrument (MIMI) on the Cassini mission to Saturn/Titan, *Space Sci. Rev.*, *114*, 233–329, doi:10.1007/s11214-004-1410-8.

Krupp, N., et al. (2009), Energetic particles in Saturn's magnetosphere during the Cassini nominal mission (July 2004–July 2008), *Planet. Space Sci.*, *57*, 1754–1768, doi:10.1016/j.pss.2009.06.010.

Kurth, W. S., A. Lecacheux, T. F. Averkamp, J. B. Groene, and D. A. Gurnett (2007), A Saturnian longitude system based on a variable kilometric radiation period, *Geophys. Res. Lett.*, *34*, L02201, doi:10.1029/2006GL028336.

McDonald, F. B., A. W. Schardt, and J. H. Trainor (1980), If you've seen one magnetosphere, you haven't seen them all: Energetic particle observations in the Saturn magnetosphere, *J. Geophys. Res.*, *85*, 5813–5830, doi:10.1029/JA085iA11p05813.

Paranicas, C., et al. (2008), Sources and losses of energetic protons in Saturn's magnetosphere, *Icarus*, *197*, 519–525, doi:10.1016/j.icarus.2008.05.011.

Randall, B. A. (1994), Energetic electrons in the magnetosphere of Saturn, *J. Geophys. Res.*, *99*, 8771–8785, doi:10.1029/94JA00254.

Roussos, E., et al. (2007), Electron microdiffusion in the Saturnian radiation belts: Cassini MIMI/LEMMS observations of energetic electron absorption by the icy moons, *J. Geophys. Res.*, *112*, A06214, doi:10.1029/2006JA012027.

Roussos, E., et al. (2008), Discovery of a transient radiation belt at Saturn, *Geophys. Res. Lett.*, *35*, L22106, doi:10.1029/2008GL035767.

Santos-Costa, D., M. Blanc, S. Maurice, and S. J. Bolton (2003), Modeling the electron and proton radiation belts of Saturn, *Geophys. Res. Lett.*, *30*(20), 2059, doi:10.1029/2003GL017972.

Schulz, M., and L. J. Lanzerotti (1974), *Particle Diffusion in the Radiation Belts*, *Phys. Chem. Space*, vol. 7, Springer, Berlin.

Simpson, J. A., T. S. Bastian, D. L. Chenette, R. B. McKibben, and K. R. Pyle (1980), The trapped radiations of Saturn and their absorption by satellites and rings, *J. Geophys. Res.*, *85*, 5731–5762, doi:10.1029/JA085iA11p05731.

Thomsen, M., and J. A. Van Allen (1980), Motion of trapped electrons and protons in Saturn's inner magnetosphere, *J. Geophys. Res.*, *85*, 5831–5834, doi:10.1029/JA085iA11p05831.

Van Allen, J. A., and C. L. Grosskreutz (1989), Relativistic electrons in Saturn's inner magnetosphere and an estimate of their synchrotron emission, *J. Geophys. Res.*, *94*, 8731–8738, doi:10.1029/JA094iA07p08731.

Walt, M. (1994), *Introduction to Geomagnetically Trapped Radiation*, doi:10.1017/CBO9780511524981, Cambridge Univ. Press, Cambridge, U. K.

T. P. Armstrong, Fundamental Technologies, LLC, 2411 Ponderosa Dr., Ste. A, Lawrence, KS 66046, USA.

P. C. Brandt, J. F. Carbary, S. M. Krimigis, D. G. Mitchell, C. Paranicas, and F. S. Turner, Johns Hopkins University Applied Physics Laboratory, 11100 Johns Hopkins Rd., Laurel, MD 20723, USA. (chris.paranicas@jhuapl.edu)

M. Burton, JPL, California Institute of Technology, 4800 Oak Grove Dr., Pasadena, CA 91109, USA.

J. F. Cooper, NASA GSFC, Greenbelt, MD 20771, USA.

K. K. Khurana and M. G. Kivelson, IGPP, UCLA, 405 Hilgard Ave., Los Angeles, CA 90095-1567, USA.

N. Krupp and E. Roussos, Max-Planck-Institut für Sonnensystemforschung, Max-Planck Str. 2, D-37191 Katlenburg-Lindau, Germany.